ELSEVIER

Structural preferences of cyclopentadienyl and indenyl rings in iridium(I) carbene complexes

Martina Prinz [a], Luís F. Veiros [b], Maria José Calhorda [c,*], Carlos C. Romão [d], Eberhardt Herdtweck [a], Fritz E. Kühn [a], Wolfgang A. Herrmann [a]

[a] *Lehrstuhl für Anorganische Chemie der Technischen Universität München, Lichtenbergstr. 4, 85747 Garching b. München, Germany*
[b] *Centro de Química Estrutural, IST, Av. Rovisco Pais, 1049-001 Lisboa, Portugal*
[c] *Departamento de Química e Bioquímica, Faculdade de Ciências da Universidade de Lisboa, 1749-016 Lisboa, Portugal*
[d] *Instituto de Tecnologia Química e Biológica, UNL, Av. da República, EAN, 2780-157 Oeiras, Portugal*

Abstract

Cleavage of the $[Ir(\eta^4\text{-COD})Cl]_2$ dimer in the presence of the corresponding imidazolium salts and the strong base $t\text{BuO}^-$ leads to the formation of Ir(I) derivatives of N-heterocyclic carbenes. When halide is replaced by NaCp, a mixture of $[Ir(\eta^4\text{-COD})(NHC^R)(\eta^1\text{-Cp})]$ and $[Ir(\eta^2\text{-COD})(NHC^R)(\eta^5\text{-Cp})]$ is obtained. The latter is favored for R = Cy, while the former predominates for R = Me. Conversely, $[Ir(\eta^4\text{-COD})(NHC^R)(\eta^1\text{-Ind})]$ is the only product of the reaction with NaInd, despite the R substituent. DFT/B3LYP calculations confirmed that the η^1 coordination mode of the ring gives rise to the most stable structures, namely square planar complexes of $5d^8$ Ir(I). The energy of the 18 electron species containing η^2-COD and η^5-Ind or Cp is higher by 13 and 5 kcal mol^{-1}, respectively. The fluxional behaviour of indenyl, detected by NMR in the solutions of $[Ir(\eta^4\text{-COD})(NHC^R)(\eta^1\text{-Ind})]$, is associated to the low energy of the η^3-Ind species required in the conversion process, and is not easily observed in the cyclopentadienyl derivatives, where a similar intermediate is disfavored.
© 2006 Elsevier B.V. All rights reserved.

Keywords: Iridium complexes; Heterocyclic carbenes; Ring hapticity; Indenyl; Cyclopentadienyl; DFT calculations

1. Introduction

Indenyl and cyclopentadienyl complexes have deserved a large amount of attention and have been widely used in synthetic chemistry, among other reasons, because of their coordination versatility, which allows for haptotropic migrations from the η^5 coordination mode, to the η^3, and finally to the η^1 one (see indenyl in Scheme 1) [1]. As each of these shifts takes place, the donor capability of the ligand decreases by two units. Therefore, addition or loss of two electrons, which can be induced either by coordination or loss of one ligand, or by a redox process, can promote such ring slippage reactions.

A perfect η^5 coordination is found in most Cp complexes, while the $\eta^3 + \eta^2$, where three M–C bonds are a bit shorter than the other two, is the rule for indenyl species [2]. As slippage occurs, the metal moves across the ring, as sketched in Scheme 1, and the ring becomes non planar (η^3). We have shown that indenyl becomes η^3 coordinated and folds much more easily than cyclopentadienyl [3]. This behaviour has been held responsible by the so-called indenyl effect, the expression coined by Basolo et al. [4], namely the acceleration of reaction rates when the Cp ligand is replaced by an indenyl. Indenyl slippage reactions were studied in detail for several Mo(II) systems, such as $[(\eta^5\text{-Ind})Mo(CO)_2L_2(NCMe)]^+$. For instance, the addition of a weakly coordinating ligand, such as NCMe, to these Mo(II) d^4 complexes leads to their conversion to $[(\eta^3\text{-Ind}Mo(CO)_2L_2(NCMe)]^+$ [5]. The dications $[(\eta^5\text{-ring})(\eta^5\text{-Ind})MoL_2]^{2+}$ (ring = Cp, Ind) can be reduced to the neutral species, $[(\eta^5\text{-ring})(\eta^3\text{-Ind})MoL_2]$.
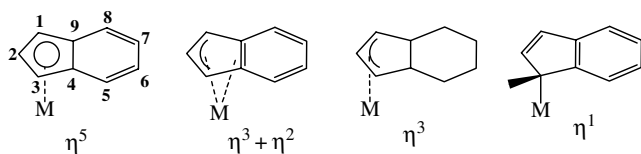
Scheme 1.

When both rings are Cp, the same reaction only takes place with strong π-acceptor carbonyls as L coligands [6]. The d^4 electron count appears to favour this haptotropic shift, being the source of many of the known examples [1b,7]. On the other hand, $\eta^5 \rightarrow \eta^3$ shifts seldom result in stable species in the case of d^6 complexes. Here, the strong drive to form octahedral (or pseudo octahedral) structures prevents ligand addition. This can be seen in the phosphine addition to $[(\eta^5\text{-Ind})\text{Mn(CO)}_3]$, the classical example of Basolo's kinetic studies, where a η^3-indenyl coordination was postulated as an intermediate, but a CO is rapidly expelled from the coordination sphere and the initial environment is recovered [4]. Computational studies fully characterized the intermediate, $[(\eta^5\text{-Ind})(\eta^3\text{-Ind})\text{Mn(PH}_3)(\text{CO})_3]$, as an unstable species [8].

The further haptotropic shift from $\eta^3 \rightarrow \eta^1$ has not been so much studied, although a review on η^1-indenyl complexes was already published in 2001 [9]. There are several examples of structurally characterized η^1-indenyl complexes and their participation as intermediates in several reactions is well documented.

In this work, the synthesis of new iridium complexes containing cyclopentadienyl or indenyl as ligands, together with a *N*-heterocyclic carbene, is described. It was found that the structural preferences in this d^8 metal center differ from those previously observed in other systems, and Cp and Ind behave differently. DFT [10] calculations were performed to understand the detected patterns, namely the structures and the fluxional behaviour in solution.

2. Results and discussion

2.1. Chemical studies – carbene precursors

The carbene complexes of type $[\text{Ir}(\eta^4\text{-COD})(\text{NHC}^R)X]$ and $[\text{Ir}(\eta^4\text{-COD})(\text{NHC}^R)_2]X$ (R = CH$_3$, X = I; R =

C_6H_{11}, X = Cl) are readily prepared by reaction of the Ir(I) dimer $[\text{Ir}(\eta^4\text{-COD})\text{Cl}]_2$ with the 1,3-dialkylimidazolium salts in the presence of a strong base as shown in Scheme 2.

The initially formed alkoxide complex deprotonates the imidazolium cation in situ, thereby avoiding the separate preparation of the free carbene [11]. The simultaneous formation of small amounts of bis-carbene complexes $[\text{Ir}(\eta^4\text{-COD})(\text{NHC}^R)_2]X$ can be decreased by using only a very small excess of imidazolium salt. These bis-carbene complexes **3** and **4** can be easily separated by column chromatography. It is worth noting that the use of imidazolium iodide leads almost exclusively to the iodo complex **1**, as already observed for similar Rh complexes [12], in agreement with the HSAB principle.

The Ir(η^4-COD)(NHC)X complexes **1** and **2** are stable in air for several days and their chromatographic purification can be performed with wet solvents in air. They are soluble in CH$_2$Cl$_2$ and THF but only slightly soluble in hexane. The main characteristics of the NMR spectra of these complexes are discussed for the cyclohexyl derivative $[\text{Ir}(\eta^4\text{-COD})(\text{NHC}^{Cy})\text{Cl}]$, **2**. In the ^{13}C NMR spectrum, the resonance of the carbene bound C atom appears at 178.4 ppm and is clearly shielded relative to that of the free ligand (δ ppm = 212.6). The resonances of the olefinic C atoms of the COD ligand appear at 83.2 and 51.1 ppm. In the ^{1}H NMR spectrum, the olefinic protons resonate at 4.46 and 2.94 ppm.

The molecular structure of **1** obtained by single crystal X-ray diffraction analysis is shown in Fig. 1 and selected bond distances and angles are given in Table 1.

The coordination around the Ir is square planar. The Ir–C1 bond distance (2.033(4) Å) is usual for this type of carbene coordination [13]. The different *trans* influences of the carbene and iodide ligands lead to different distances between the coordinated COD carbon atoms and the Ir. As a result of the longer distance to the metal, the C12=C13 double bond *trans* to the NHC^{Me} ligand is shorter [1.389(7) Å] than the C8=C9 bond [1.424(7) Å], owing to reduced backdonation from the metal to its π^* orbitals.
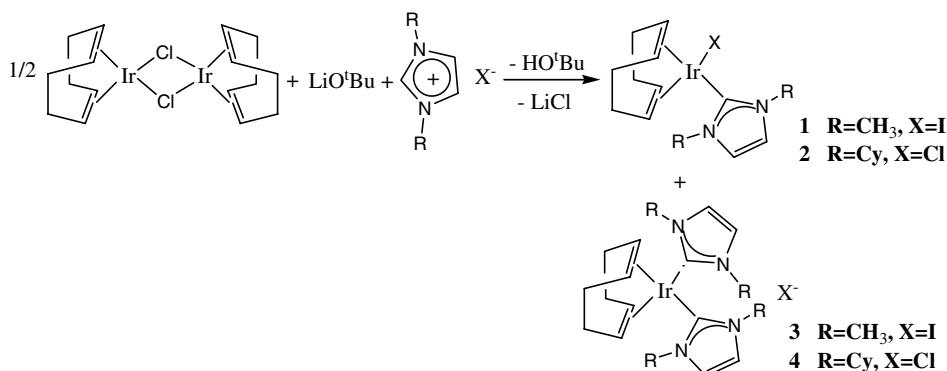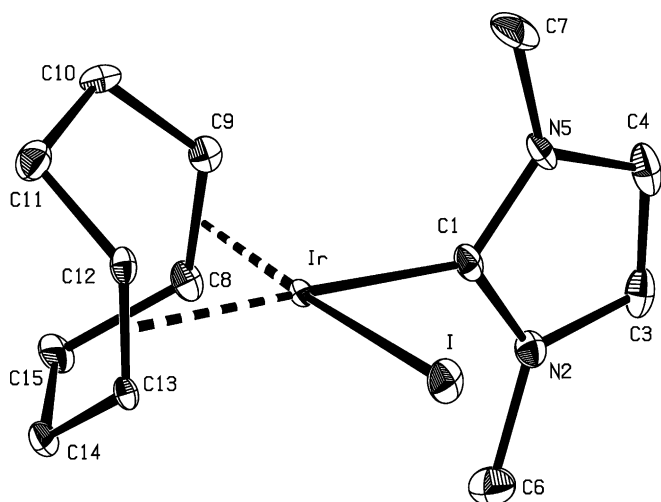

Scheme 2.

Fig. 1. ORTEP diagram and atom numbering scheme of [Ir(η^4-COD)(NHC^{Me})I] (1) (ellipsoids with 50% probability, hydrogen atoms are omitted for clarity).

Table 1
Selected distances (Å) and angles (°) of [Ir(η^4-COD)(NHC^{Me})I] (1)

Distance[a]		Angle[a]	
Ir–I	2.6694(3)	I–Ir–C1	88.9(1)
Ir–C1	2.033(4)	I–Ir–C8	163.5(1)
Ir–C8	2.122(4)	I–Ir–C9	157.0(1)
Ir–C9	2.096(4)	I–Ir–C12	94.5(1)
Ir–C12	2.197(4)	I–Ir–C13	92.7(1)
Ir–C13	2.176(5)	I–Ir–Cg1	176.9
Ir–Cg1	1.985	I–Ir–Cg2	93.8
Ir–Cg2	2.073	C1–Ir–C8	91.3(2)
C8–C9	1.424(7)	C1–Ir–C9	89.6(2)
C12–C13	1.389(7)	C1–Ir–C12	163.9(2)
		C1–Ir–C13	158.6(2)
		C1–Ir–Cg1	90.5
		C1–Ir–Cg2	176.2
		N2–C1–N5	104.6(4)

[a] Cg1, Cg2: mid-points of C8–C9 and C12–C13.

The bis-carbene complexes **3** and **4** are obtained, in small amounts, in the column chromatographic purification of **1** and **2**, respectively. Their formation corresponds to the reaction depicted in Scheme 3. In spite of its ionic nature, **3** is exclusively formed with the I$^-$ counter ion as indicated by elemental analysis.

These air stable complexes are very soluble in CH$_2$Cl$_2$, but only moderately soluble in THF. The ^{13}C NMR spectrum of [Ir(η^4-COD)(NHC^{Cy})$_2$]Cl, **4**, presents the resonance of the carbene Ir bound C atoms at 174.7 ppm.

The resonances of the olefinic ligands are observed at 76.6 ppm in the ^{13}C NMR spectrum, and at 3.82 ppm in the ^{1}H NMR spectrum for the corresponding protons. Both cations of **3** and **4** are observed in the FAB mass spectrum (see Section 4).

### 2.2. Chemical studies – cyclopentadienyl and indenyl complexes of the type [Ir(η^5-ring)(NHC^{Me})]

Reaction of **1** with NaCp in THF takes place between 0 and 25 °C to give a mixture of the carbene complexes **5** and **6** in a 94/6 ratio as ascertained by ^{1}H NMR of the crude reaction product (Scheme 4).

Crystallization from CH$_2$Cl$_2$/hexane leads to separation of both products. [Ir(η^4-COD)(η^1-Cp)(NHC^{Me})], **5**, is air sensitive. The ^{13}C NMR spectrum shows resonances of the carbene C atom at 186.5 ppm, the Cp ligand at 109.1 ppm, and the olefinic C atoms of the COD ligand at 77.7 and 51.4 ppm. In the ^{1}H NMR spectrum, a signal at 5.64 ppm is assigned to the Cp protons of the η^1-Cp ligand. The olefinic protons appear at 4.31 and 2.81 ppm. Crystals were grown by diffusion of *n*-hexane into a saturated solution of CH$_2$Cl$_2$, and their crystal structure was determined by X-ray diffraction (Fig. 2). Selected distances and bond angles are given in Table 2.

The Ir coordination is square planar with the sum of the angles around the Ir deviating only 0.16° from the 360° value. The Ir–C1 (carbene) distance (2.035(7) Å) is normal for an Ir–C single bond. The folding angle between the planes defined by C6, C7, C10 and C8, C9 atoms of the Cp ligand is $\Omega = 3(1)°$. As discussed for the structure of **1**, the C=C distances of the COD ligand are different (C14–C15 = 1.397(10) Å; C11–C18 = 1.418(10) Å), reflecting the different *trans* influences of the carbene and η^1-Cp ligands, also shown in the Ir–C distances to both double bonds.

According to this structure, **5** is clearly classified as a 16e complex. Surprisingly, the 18 e by-product **6** shown in Scheme 4, is formed in small amounts (**5**:**6** = 94:6). It was characterized by ^{1}H NMR in CD$_2$Cl$_2$, owing to its very typical singlet originating from the η^5-Cp ligand, and the clearly different resonances of the free and coordinated double bonds of the η^2-COD ligand, in agreement with the fully characterized analogue **7** (see below).

The reason for this preference for an unsaturated electronic structure at Ir(I) was not completely traceable in the beginning. The presence of steric factors seemed to play
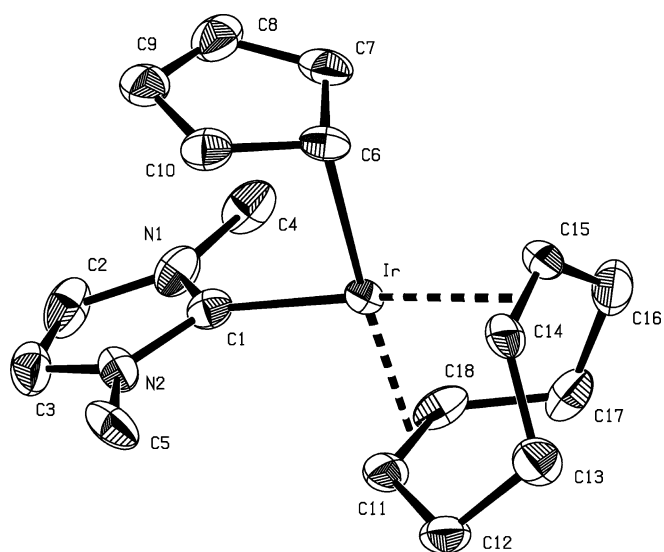

3 R=CH$_3$, X=I
4 R=Cy, X=Cl
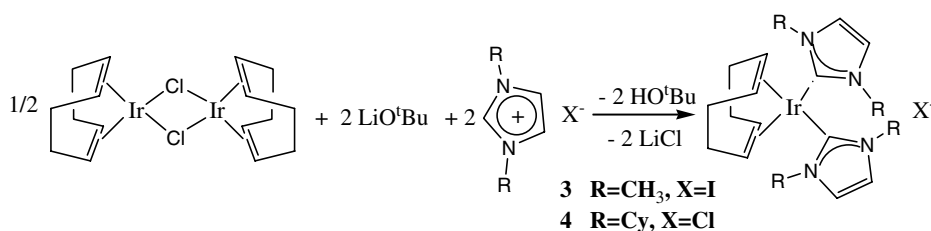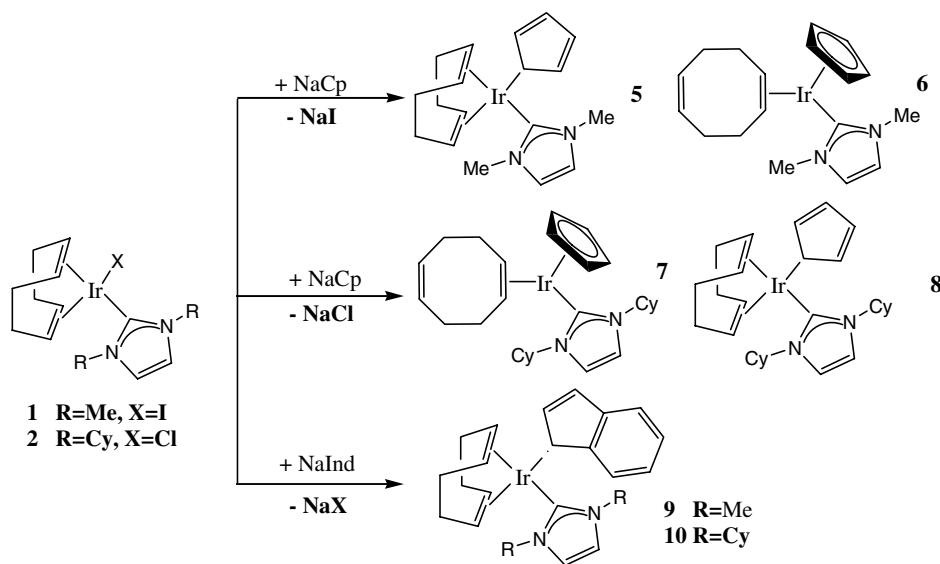
Scheme 3.

Scheme 4.

Fig. 2. ORTEP diagram and atom numbering scheme of $[Ir(\eta^4\text{-COD})(\eta^1\text{-Cp})(NHC^{Me})]$ (5) (ellipsoids with 50% probability, hydrogen atoms are omitted for clarity).

Table 2
Selected distances (Å) and angles (°) of $[Ir(\eta^4\text{-COD})(\eta^1\text{-Cp})(NHC^{Me})]$ (5)

Distance[a]		Angle[a]	
Ir–C1	2.035(7)	C1–Ir–C6	96.5(3)
Ir–C6	2.199(7)	C1–Ir–Cg1	89.2
Ir–C11	2.117(7)	C1–Ir–Cg2	175.1
Ir–C14	2.194(7)	C6–Ir–Cg1	173.8
Ir–C15	2.176(7)	C6–Ir–Cg2	88.2
Ir–C18	2.135(7)	N1–C1–N2	104.3(6)
Ir–Cg1	2.004		
Ir–Cg2	2.070		
C11–C18	1.418(10)		
C14–C15	1.397(10)		

[a] Cg1, Cg2: mid-points of C11–C18 and C14–C15.

a role since the facile substitution in Scheme 4 does not take place with the bulkier Cp* ligand (from LiCp*). In order to probe steric effects, the reaction of **2**, which bears a much bulkier Cy substituent at the NHC ligand, with NaCp was carried out. In this case, the main product was the 18 e η^5-Cp complex **7**, formed in a 86:14 ratio relative to the 16 e tautomer **8**. **7** is air sensitive, soluble in CH_2Cl_2, and insoluble in hexane. The resonance of the carbene carbon atom appears at 159.5 ppm in the ^{13}C NMR spectrum. In the ^1H and ^{13}C NMR spectra both resonances of the protons (δ ($C_5H_5 = 4.80$ ppm)) and carbons (δ ($C_5H_5 = 76.8$ ppm)) of the Cp ligand are shifted to higher fields, relative to the corresponding signals in **5**: δ ($C_5H_5 = 5.64$ ppm) and δ ($C_5H_5 = 109.1$ ppm). A similar high field shift is also observed for the CH signals of the olefinic bonds coordinated to the Ir: δ (C$H = 37.6$ ppm). Such high field shifts certainly originate from the different coordination modes of the Cp ligand in both **5** (η^1-Cp) and **7** (η^5-Cp). The signals of the CH-olefinic protons reflect their different coordination situation: δ (C$H = 2.43$ ppm) for the coordinated HC=CH and δ (C$H = 5.56$ ppm) for the free HC=CH. In accordance, the respective ^{13}C chemical shifts are also clearly different: δ (C$H = 37.6$ ppm) for coordinated HC=CH and δ (C$H = 131.1$ ppm) for the free HC=CH bond. The minority reaction product **8** shows NMR data for the Cp and olefin atoms very similar to those of **5** (δ (C_5H_5) = 5.74 ppm and δ (C_5H_5) = 110.3 ppm), allowing for the ready quantification of the **7**:**8** ratio. The spectroscopic features of **7** are in accordance with the structural data obtained by single crystal X-ray diffraction, as seen in Fig. 3. Selected distances and bond angles are given in Table 3.

The iridium exhibits a distorted pseudotrigonal planar coordination. The Ir–C1 (carbene) bond is typical for an Ir–C single bond (1.987(5) Å) [13]. The coordination of the Cp ligand is clearly η^5 with the Ir–C$_{Cp}$ bond lengths
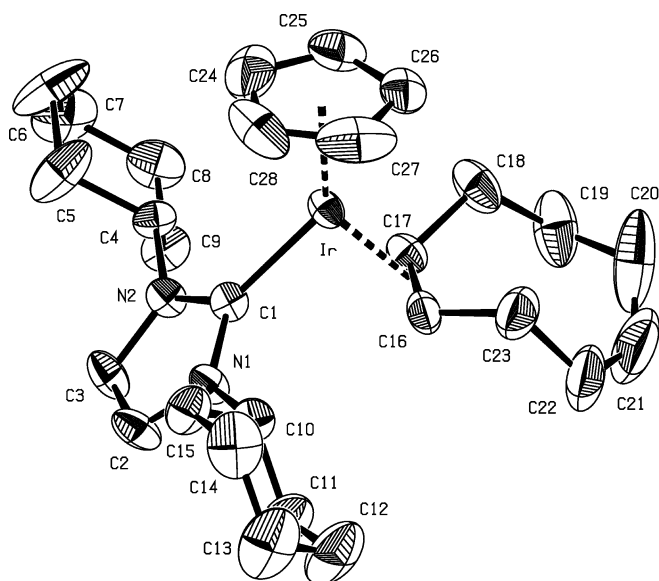
Fig. 3. ORTEP diagram and atom numbering scheme of [Ir(η^2-COD)(η^5-Cp)(NHC^{Cy})] (**7**) (ellipsoids with 50% probability, hydrogen atoms are omitted for clarity).

Table 3
Selected distances (Å) and angles (°) of [Ir(η^2-COD)(η^5-Cp)(NHC^{Cy})] (**7**)

Distance[a]		Angle[a]	
Ir–C1	1.987(5)	C1–Ir–C16	86.3(2)
Ir–C16	2.093(6)	C1–Ir–C17	89.2(2)
Ir–C17	2.101(6)	C1–Ir–Cg1	132.2
Ir–C24	2.292(9)	C1–Ir–Cg2	87.6
Ir–C25	2.275(7)	Cg1–Ir–Cg2	140.2
Ir–C26	2.223(5)	N1–C1–N2	104.2(5)
Ir–C27	2.248(7)		
Ir–C28	2.240(8)		
C16–C17	1.453(10)		
Ir–Cg1	1.918		
Ir–Cg2	1.967		

[a] Cg1: centroid of the Cp-ligand and Cg2: mid-point of C16–C17.

between 2.223(5) and 2.292(9) Å. The η^2-coordination of the COD is evident and C=C coordinated double bond is longer [1.453(10) Å] than the free C=C bond [1.36(2) Å], reflecting back donation from an electron-rich low valent Ir center.

This subtle variation of the Cp ring coordination mode is not so commonly observed, being more readily present in Indenyl complexes. Therefore, we decided to compare both systems in order to try to assign the reasons for this behavior.

According to the chemistry in Scheme 4, the use of NaInd instead of NaCp led to the preparation of the complexes [Ir(η^4-COD)(NHC^R)(η^1-Ind)], for both R = Me (**9**), Cy (**10**). The hapticity in this formulation results from the X-ray crystal diffraction analysis of **10**, shown in Fig. 4. Selected distances and bond angles are given in Table 4.

The structure is similar to that of the analogous Cp complex **5**. The square planar arrangement around the Ir(I) centre is reflected in the sum of the angles, which amounts exactly to 360°. The bond distances relative to Ir–carbene

[2.053(5) Å] and to the C=C and C–Ir bonds of the COD ligand have the same features already discussed above for **5**. The η^1-C–Ir distance is 2.187(5) Å and the folding angle (between planes C16, C24, C23 and C16, C17, C22, C23) of the indenyl is $\Omega = 7(1)°$.

More interesting is the fluxional behavior in solution. In the ^{1}H NMR spectrum at 25 °C, the olefinic CH protons of the COD ligand produce only one broad resonance at $\delta = 3.05$ ppm and the H1 and H3 protons of the indenyl appear as a doublet at δ 5.48 ppm (see numbering of the indenyl protons in Scheme 1, above). Upon cooling, the resonance of the olefinic COD protons broadens and splits into two resonances at δ 3.02 and 2.90 ppm with a coalescence temperature of −20 °C. Further cooling results in a shift of the resonance at 3.02 ppm to higher field until it disappears under the signal at 2.89 ppm (Fig. 5, left). The doublet of the H1, H3 indenyl protons, shifts to lower field, broadens and eventually disappears as a very broad signal at ca. −100 °C (Fig. 5, right).

In the ^{13}C NMR spectrum at 25 °C, the signal of the carbene carbon appears at 185.0 ppm, but the resonances of the olefinic COD carbons at 35 °C are either hidden under the solvent signals or too broad to be recognized. Upon cooling two new resonances appear at ca. 0 °C (Fig. 6).

The resonance of the quaternary C4 and C9 atoms of the indenyl ring at 148.9 ppm indicates a η^3-Ind coordination mode, according to the correlation between indenyl hapticity and C4/C9 chemical shifts established by Baker and Tulip [14]. Lowering the temperature causes this signal to broaden and eventually disappear at ca. −100 °C. The resonances of the C1 and C3 atoms of the indenyl ring that appear at 86.8 ppm, and are already broad signals at 25 °C, disappear on cooling at ca. −50 °C.

This fluxional behavior in solution can be accommodated by the set of equilibria between 16e and 18e species depicted in Scheme 5. The equilibrium between species A and B corresponds to a change in hapticity $\eta^1 \rightarrow \eta^3$ also allowed by the 18e rule. The equilibrium between B and C represents an alternative way of exchanging between 18e and 16e species, which is to expect in a very electron-rich species as B. The equilibrium between C and D might be caused by the same driving force (EAN configuration) and has been observed in several cases on ring-slippage of the indenyl ring [1,7].

2.3. DFT calculations

DFT [10] calculations were performed in order to understand the structural preferences of the Cp and Ind complexes of the Ir(COD)(NHC^R) fragment and the fluxional behaviour of the indenyl complex in solution, as observed in the ^{1}H and ^{13}C NMR results. The carbene substituents were replaced by hydrogen atoms.

Three different geometries were obtained from the optimization of [Ir(COD)(Ind)(NHC^H)] (Fig. 7). One corresponds to the X-ray structure determination (**10**), with the indenyl exhibiting a η^1 coordination mode, and is the
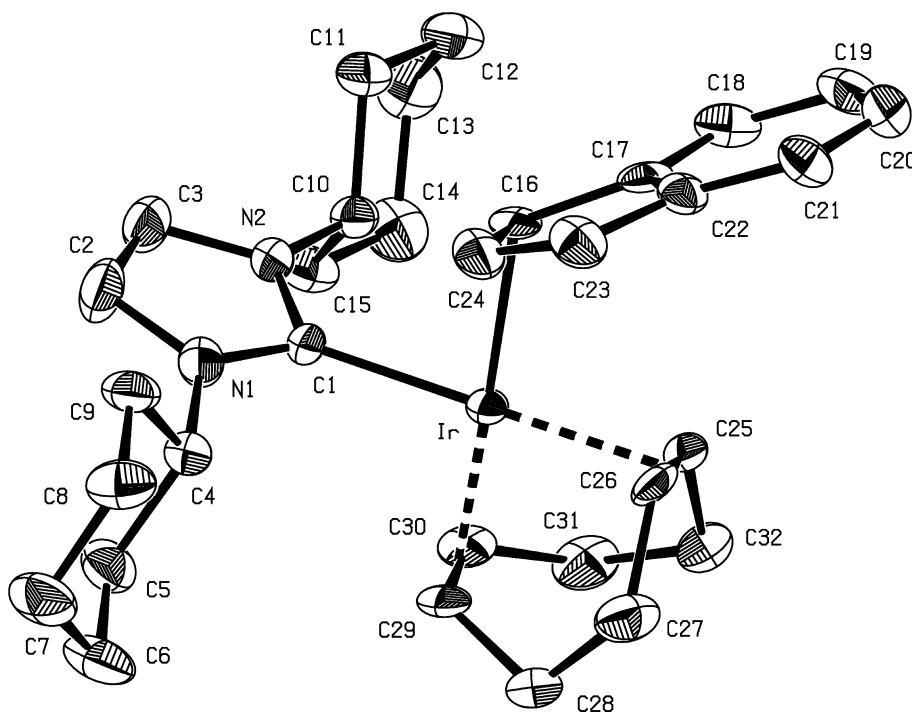
Fig. 4. ORTEP diagram and atom numbering scheme of $[Ir(\eta^4\text{-COD})(NHC^R)(\eta^1\text{-Ind})]$ (**10**) (ellipsoids with 50% probability, hydrogen atoms are omitted for clarity).

Table 4
Selected distances (Å) and angles (°) of $[Ir(\eta^4\text{-COD})(NHC^R)(\eta^1\text{-Ind})]$ (**10**)

Distance[a]		Angle[a]	
Ir–C1	2.053(5)	C1–Ir–C16	84.2(2)
Ir–C16	2.187(5)	C1–Ir–Cg1	179.6
Ir–C25	2.191(5)	C1–Ir–Cg2	93.9
Ir–C26	2.172(5)	C16–Ir–Cg1	95.4
Ir–C29	2.136(5)	C16–Ir–Cg2	178.1
Ir–C30	2.144(6)	Cg1–Ir–Cg2	86.5
Ir–Cg1	2.071	N1–C1–N2	104.6(4)
Ir–Cg2	2.018		
C25–C26	1.369(7)		
C29–C30	1.425(9)		

[a] Cg1, Cg2: mid-points of C25–C26 and C29–C30.

most stable by 13 kcal mol^{-1}. The other two species are iso-energetic and include a η^3-Ind piano stool complex and a η^5-Ind complex with a η^2 coordinated cyclooctadiene and an overall geometry similar to the X-ray structure of the Cp complex **7**.

The geometry calculated for $[Ir(\eta^1\text{-Ind})(\eta^4\text{-cod})(carbene)]$ (Fig. 7, left) shows a square planar environment around the metal coordination sphere, as described in the X-ray crystal structure obtained for complex **10**. The calculated metal–ligand bond distances [for instance Ir–C(Ind) = 2.194 Å, Ir–C(carbene) = 2.026 Å and Ir–C(cod) = 2.154–2.216 Å] are in very good agreement with the experimental ones [Ir–C(Ind) = 2.188 Å, Ir–C(carbene) = 2.051 Å and Ir–C(cod) = 2.133–2.188 Å], and the Ind folding angle is $\Omega = 7°$, both in the experimental and the calculated structure.

The optimized geometry of the η^3-Ind complex $[Ir(\eta^4\text{-COD})(\eta^3\text{-Ind})(NHC^H)]$ (Fig. 7, centre) corresponds to a piano stool arrangement with a clearly folded indenyl (folding angle $\Omega = 23°$), and two types of Ir–C(Ind) distances: three within bonding values (2.103, 2.268 and 2.351 Å) and two much larger ones, corresponding to the hinge carbons C4 and C9 (3.056 and 3.096 Å), characterizing the η^3 coordination of the ligand. A similar structure has been reported by Merola et al. for $[Ir(\eta^3\text{-Ind})(PPhMe_2)_3]$ [15] and displays the largest indenyl folding known up to date ($\Omega = 27°$). Both are related to the calculated structure of the isoelectronic $[Mn(\eta^3\text{-Ind})(CO)_3]^{2-}$ ($\Omega = 17°$) [16]. The calculated Ir–C(COD) (2.145–2.193 Å) and Ir–C(carbene) (2.147 Å) distances are similar in the two structures containing η^1- and η^3-Ind, although the slightly longer Ir–C(carbene) bond length (0.121 Å) in the η^3-Ind complex probably reflects the more crowded metal coordination sphere.

The third indenyl complex $[Ir(\eta^2\text{-COD})(\eta^5\text{-Ind})(NHC^H)]$ (Fig. 7, right) is analogous to the cyclopentadienyl complex **7**, $[Ir(\eta^5\text{-Cp})(\eta^2\text{-cod})(carbene)]$, with a pseudo triangular environment around Ir, defined by the carbene carbon atom, the Cp centroid and the middle of the coordinated C=C bond of COD. The calculated Ir–C(COD) (2.104 and 2.132 Å) and Ir–C(carbene) (1.959 Å) distances are very close to those experimentally determined for **7** (Ir–C = 2.093 and 2.101 Å, and 1.987 Å, respectively).

Indenyl is coordinated to iridium by the five carbon atoms, with bonding distances ranging between 2.244 and 2.597 Å, but there are three shorter (2.244, 2.264,
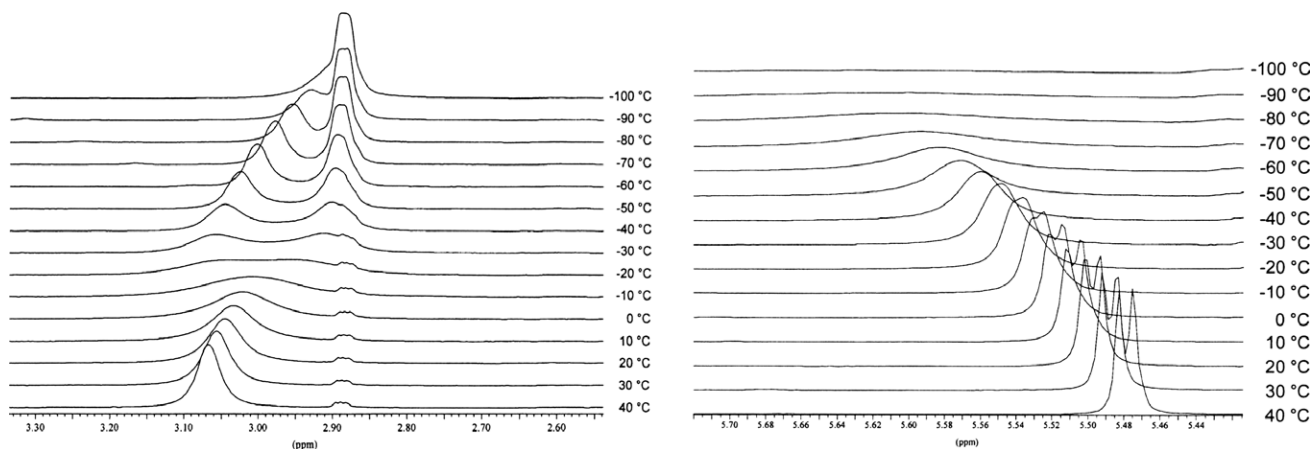
Fig. 5. Temperature dependence of the ^{1}H NMR protons of the olefinic protons of COD (left) and the H1/H3 protons of the indenyl ligand (right).
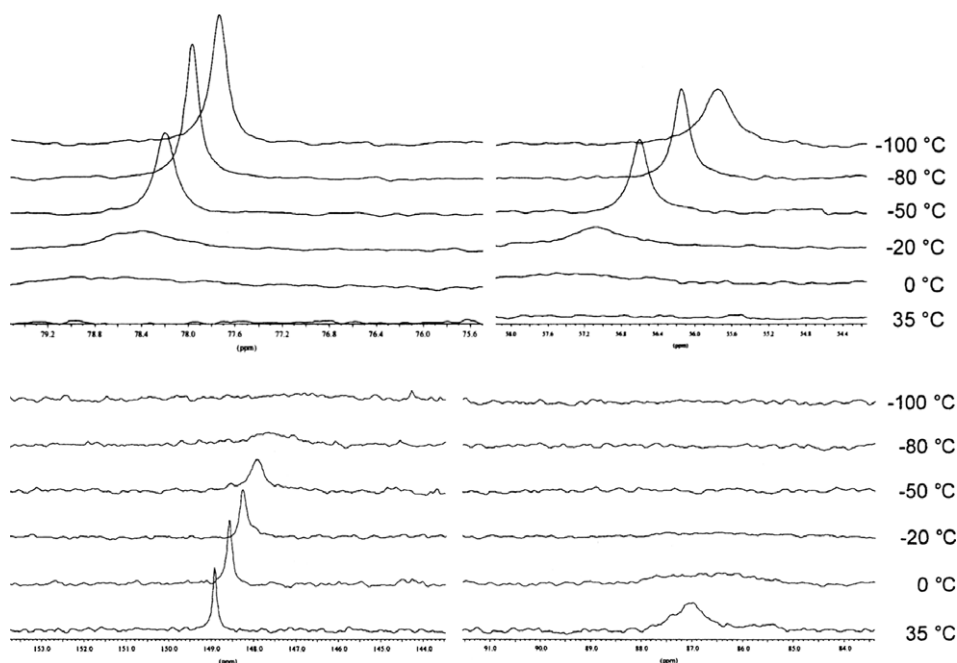
Fig. 6. Temperature dependence of the ^{13}C NMR protons of the olefinic carbons of COD (left) and the C4/C9 and C1/C3 carbons of the indenyl ligand (right).
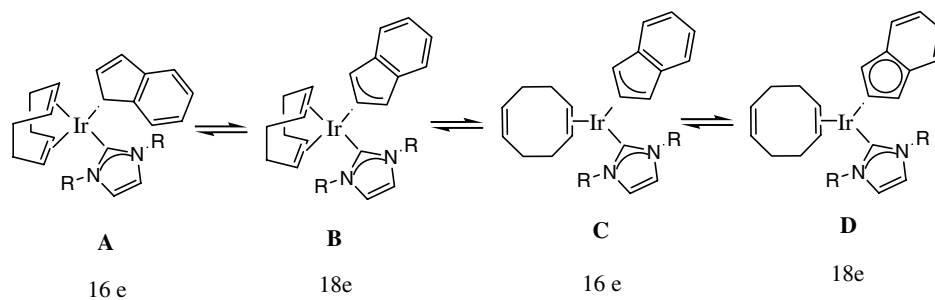
Scheme 5.

2.333 Å) and two longer Ir–C distances (2.545, 2.597 Å), corresponding to the hinge carbons, with a folding angle $\Omega = 9°$, defining a "$\eta^3 + \eta^2$" coordination of the indenyl ligand [7a].

An energy difference of 13 kcal mol^{-1} between the three species is in agreement with the fluxional behaviour observed by NMR in solution. An equilibrium between the η^5 and the η^1 complexes may exist in solution, shifted

Fig. 7. Optimized geometries of [Ir(η^m-COD)(η^n-Ind)(NHC^H)] complexes with some relevant distances (Å), folding angle (italics, °) and the relative energies (kcal mol^{-1}). Left: $n = 1$, $m = 4$; centre: $n = 3$, $m = 4$; right: $n = 5$, $m = 2$.
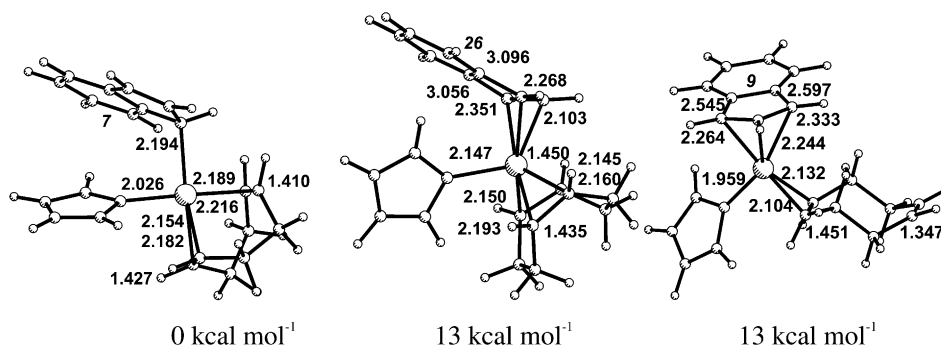
towards the latter. Indeed, an indenyl η^1 to η^3 haptotropic shift, accompanied by a geometry rearrangement of the complex, could lead to the η^3-Ind species, and from that to [Ir(η^5-Ind)(η^2-cod)(carbene)] via a η^3 to η^5 indenyl shift and the opening of the Ir–C bonds to one C=C in cyclooctadiene ($\Delta E \approx 0$) (Fig. 7).

The preference of the η^1-Ind complex for the square planar geometry is easily traced to the d^8 electron configuration of Ir(I) and the stability of the 16 electron species. The other two species, η^3-Ind and η^5, are 18 electron species with other geometries [17].

In view of these results, it was puzzling that the complex [Ir(η^3-Ind)(PPhMe$_2$)$_3$] [15] mentioned above had an 18 electron count. Therefore, both its geometry and that of an η^1-Ind isomer were fully optimized (Fig. 8), using PH$_3$ as model for the phosphine. Indeed, the square planar geometry of the η^1-Ind complex is 3 kcal mol^{-1} more stable than the experimental one.

The small energy difference between the two isomers indicates only a small electronic preference for the square planar, while the phenyl groups, not taken into account in the model, will shift the balance towards the pseudo tetrahedral η^3 species [15]. The geometry obtained for [Ir(η^3-Ind)(PH$_3$)$_3$] is in good agreement with the experimental one.

The cyclopentadienyl ring in **5** and **7** behaved in a different way. Thus, a parallel study was carried out for the Cp

complexes. Only two structures, corresponding to **5** and **7** were obtained (Fig. 9). No Cp equivalent of the folded η^3-Ind complex could be optimized.

In the η^1-Cp complex (Fig. 9, left) the square planar geometry around Ir is found as in the indenyl complex and in the X-ray crystal structure of **5**. Both the optimized bond distances and the fold angle are very close to the experimental ones (Ir–C(Cp) = 2.202 Å, Ir–C(carbene) = 2.031 Å, Ir–C(COD) = 2.107–2.186 Å, $\Omega = 3°$).

The η^5-Cp complex (Fig. 9, right), has a pseudo triangular geometry around the metal, as the indenyl analogue and the X-ray crystal structure of **7**. The calculated distances and the folding angle agree very well with the experimental ones (Ir–C(Cp) = 2.223–2.292 Å, Ir–C(carbene) = 1.987 Å, Ir–C(COD) = 2.093 and 2.101 Å, $\Omega = 3°$). One difference from the η^5-Ind analogue consists in the narrow range of the IrC(Cp) distances, which differ by only 0.04 (calculated) and 0.07 Å (experimental), in comparison to 0.353 Å, as calculated for η^5-Ind in [Ir(η^2-COD)(η^5-Ind)(NHC^H)]. The coordination of the Cp is indeed η^5, while for the indenyl it is better described as $\eta^3 + \eta^2$ (see above). On the other hand, the preference for η^1-Cp over η^5-Cp is only 5 kcal mol^{-1}, compared to 13 in the related indenyl complexes. This explains why two isomers could be isolated for the Cp system (**5** and **7**), but only one for the indenyl case (**10**), and reflects the known enhanced thermodynamic stability of η^5-Cp relative to η^5-Ind. This results from a
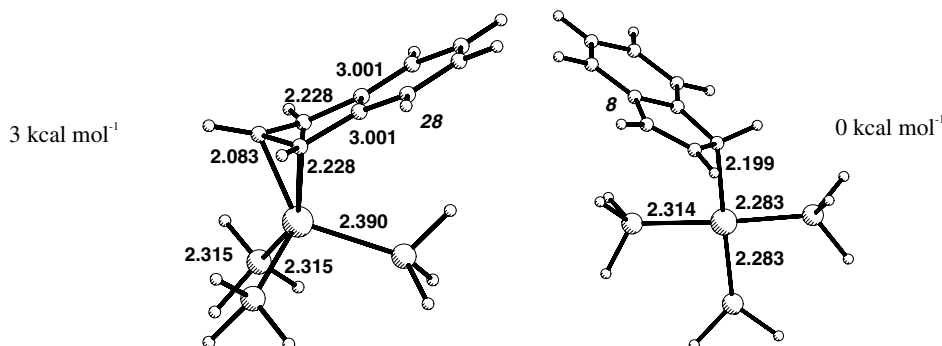

Fig. 8. Optimized geometries of [Ir(η^3-Ind)(PH$_3$)$_3$] (left) and [Ir(η^1-Ind)(PH$_3$)$_3$] (right) with some relevant distances (Å), folding angle (italics, °) and the relative energies (kcal mol^{-1}).

Fig. 9. Optimized geometries of $[Ir(\eta^4$-COD$)(\eta^1$-Cp$)(NHC^H)]$ (left) and $[Ir(\eta^2$-COD$)(\eta^5$-Cp$)(NHC^H)]$ (right) with some relevant distances (Å), folding angle (italics, °) and the relative energies (kcal mol^{-1}).
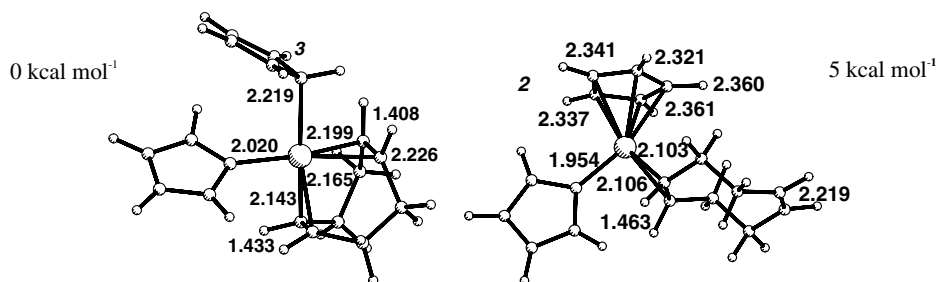
stronger bond to the metallic fragment, and is shown, for instance, by the different coordination modes, η^5-Cp vs. $\eta^3 + \eta^2$-Ind, and by the mean Ir–C distances: 2.34 and 2.40 Å for the Cp and the Ind complexes, respectively [6,8,16].

For the same reason, the absence of an η^3-Cp intermediate should make any interconversion equilibrium between the two isomers more difficult. This suggests a much higher energy barrier connecting the η^5-Cp and the η^1-Cp species. η^3-Cp complexes are unusual, as a consequence of the difficulty of cyclopentadienyl to slip and fold from η^5 to η^3, as compared to indenyl [18].

Another interesting aspect concerns the indenyl conformation with respect to the Ir(COD) fragment in the optimized structure obtained for $[Ir(\eta^1$-Ind$)(\eta^4$-COD$)$-(carbene)], where it lies over the carbene (Fig. 10). This is the experimentally observed conformation found in the η^1-Cp complex **5**, but is the opposite of the conformation determined for complex **10**, where the ligand lies over the cyclooctadiene. This results from the interligand repulsion, and is a direct consequence of the models used in the calculations, in which the real carbene N-substituents (Cy and Me) were replaced by hydrogen atoms. The first arrangement, with the indenyl over the carbene, is slightly more stable, by 5 kcal mol^{-1}. While the Me substituent on the carbene can coexist with the η^1-Ind ligand, the bulkier Cy present in complex **10** pushes the indenyl away, placing it over the COD. The overall geometrical features are equivalent for the two conformers. In particular, the bond distances are very close (Fig. 10), but the enhanced repulsion between the COD and the indenyl ligands is reflected in the less stable isomer by slightly longer Ir–C(COD) and Ir–C(Ind) distances.

The carbene substituents also influence the orientation of this ligand, which tends to be horizontal (parallel to the π ligand, Cp or Ind) in the X-ray crystal structures of **5**, **7**, and **10**, but becomes almost vertical in some calculated structures, such as $[Ir(\eta^2$-COD$)(\eta^5$-Cp$)(NHC^H)]$ (Fig. 9, right).

Experimental [19] and theoretical [20] evidence has suggested that no strong π component exists in the bonding of a N-heterocycle carbene to a transition metal centre; as no electronic effects determine its orientation, free rotation around the M–C(carbene) bond is expected. Thus, in the complexes studied, the orientation of the carbene relative to other ligands reflects steric constraints, namely interligand repulsion.

3. Conclusions

Ir(I) derivatives of N-heterocyclic carbenes (NHC^R) are readily prepared upon cleavage of the dimer $[Ir(\eta^4$-COD$)Cl]_2$ in the presence of the corresponding imidazolium salts and the strong base tBuO$^-$. Replacement of the halide by NaCp leads to mixtures of $[Ir(\eta^4$-COD$)(NHC^R)(\eta^1$-Cp$)]$ and $[Ir(\eta^2$-COD$)(NHC^R)(\eta^5$-Cp$)]$. The latter is favored for R = Cy, while the former predominates for R = Me. In contrast, the similar reaction with NaInd leads only to $[Ir(\eta^4$-COD$)(NHC^R)(\eta^1$-Ind$)]$ for both R substituents. However, they are fluxional in solution. DFT calculations showed that indeed the η^1-Cp or η^1-Ind complexes are the most stable species, but the
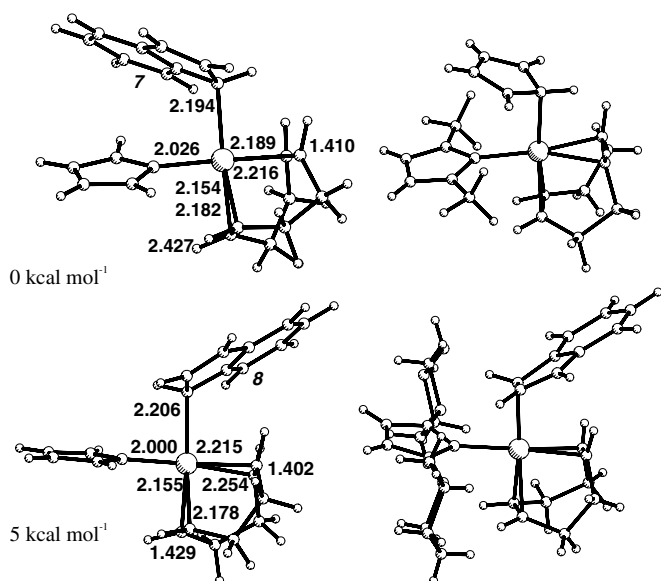
Fig. 10. Optimized geometries of two conformers of $[Ir(\eta^4$-COD$)(\eta^1$-Ind$)(NHC^H)]$ with the indenyl ring over the carbene (left, top) and over the COD (left, bottom), with some relevant distances (Å), folding angle (italics, °) and relative energies (kcal mol^{-1}). Experimental structures of $[Ir(\eta^4$-COD$)(\eta^1$-Cp$)(NHC^{Me})]$ (right, top) and $[Ir(\eta^4$-COD$)(\eta^1$-Ind$)$-$(NHC^{Cy})]$ (right, bottom).

energy of η^5-Cp is only 5 kcal mol^{-1} higher, while that of η^5-Ind differs by 13 kcal mol^{-1}. Therefore, the two coordination modes are observed for Cp, but not for Ind. On the other hand, the energy of the 18 electron η^3-Ind complex is the same as the energy of the η^5-Ind, so that a fluxional behaviour can be observed. This is not expected for the Cp ring, as η^3-Cp coordination is much less favored.

4. Experimental

All experiments were performed under inert atmosphere (N$_2$) using standard Schlenk techniques, unless otherwise stated. Solvents were degassed and dried according to the procedure described in Ref. [21] The ^{1}H and ^{13}C NMR spectra were recorded at 399.78 and 100.5 MHz, respectively, on a FT-JEOL GX 400 instrument. Elemental analysis was performed by Mr. R. Barth at the analytical laboratory of the TUM. Mass spectra were obtained with Finnigan MAT 311 A and a MAT 90 spectrometers.

4.1. General preparation of the complexes [Ir(η^4-COD)(NHC^R)X] (1, 2, 3, 4)

A solution of [Ir(η^4-COD)Cl]$_2$ dissolved in THF was treated with LiOBu^t (1.5 eq./Ir). The initial solution loses transparency and darkens. After 30 min of stirring at 25 °C, 1,3-dialkylimidazolium halide (1.1 eq./Ir) is added and the mixture left stirring for 60 h at 25 °C. The solvent is removed under vacuum and the crude product purified by column chromatography on silica-gel 60 using a mixture of CH$_2$Cl$_2$/MeOH as eluent.

4.2. (η^4-1,5-cyclooctadiene)-(iodo)-1,3-dimethylimidazoline-2-ylidene)-iridium(I) (1)

Reagents. 845 mg (1.26 mmol) [Ir(η^4-COD)Cl]$_2$; 30 mL THF; 302 mg (3.77 mmol, 1.5 eq./Ir) LiOBu^t, 620 mg (2.77 mmol, 1.1 eq./Ir) 1,3-dimethylimidazolium iodide, Yield: 1.165 g (88.5%) golden brown powder.

Anal. Calc. for C$_{13}$H$_{20}$IN$_2$Ir (523.439): C 29.83, H 3.85, N 5.35, I 24.24. Found: C 29.62, H 3.60, N 5.15, I 24.50, Cl < 0.9%.

^{1}H NMR (CD$_2$Cl$_2$, 25 °C): $\delta = 6.87$ (s, 2H, NCHCHN), 4.65 (s, 2H, CH$_{cod}$), 3.83 (s, 6H, NCH$_3$), 3.01 (s, 2H, CH$_{cod}$), 2.10 (m, 4H, CH$_{2cod}$), 1.75 (m, 2H, CH$_{2cod}$), 1.38 (m, 2H, CH$_{2cod}$). ^{13}C NMR (CD$_2$Cl$_2$, 25 °C): $\delta = 180.4.$ (NCN), 122.1 (NCHCHN), 82.3 (CH$_{cod}$), 54.7 (CH$_{cod}$) (Signal at 135°-DEPT NMR), 37.5 (NCH$_3$), 33.2 (CH$_{2cod}$), 30.7 (CH$_{2cod}$). MS (CI; m/z): 524 [M$^+$ (correct isotopic pattern).

4.3. (Chloro)-(1,3-dicyclohexylimidazoline-2-ylidene)-(η^4-1,5-cyclooctadiene)-iridium(I) (2)

Reagents. 830 mg (1.24 mmol) [Ir(η^4-COD)Cl]$_2$; 230 mL THF; 397 mg (3.71 mmol, 1.5 eq./Ir) LiOBu^t; 731 mg (2.72 mmol, 1.1 eq./Ir) 1,3-Dicyclohexylimidazolium chloride.Yield: 1.246 g (88.8%) yellow powder.

Anal. Calc. for C$_{23}$H$_{26}$ClN$_2$Ir (568.224): C 48.62, H 6.39, N 4.93, Cl 6.24. Found: C 49.06, H 6.55, N 4.60, Cl 5.96.

^{1}H NMR (CD$_2$Cl$_2$, 25 °C): $\delta = 6.89$ (s, 2H, NCHCHN), 5.10 (m, 2H, CH$_{cy}$), 4.46 (m, 2H, CH$_{cod}$), 2.94 (m, 2H, CH$_{cod}$), 2.40–1.00 (m, 28H, CH$_{2cy}$ and CH$_{2cod}$).

^{13}C NMR (CD$_2$Cl$_2$, 25 °C): $\delta = 178.4$ (NCN), 117.3 (NCHCHN), 83.2 (CH$_{cod}$), 60.3 and 51.1 (CH$_{cy}$ and CH$_{cod}$), 34.6, 34.2, 34.1, 30.0, 26.4, 26.2, 25.8 (CH$_{2cy}$ and CH$_{2cod}$).

MS (CI; m/z): 568 [M$^+$] (correct isotopic pattern), 233 [carbene + H$^+$].

From the chromatography the two (η^4-1,5-cyclooctadiene)-bis(1,3-dimethylimidazoline-2-ylidene)-iridium(I) halides 3 and 4 obtained are pure.

4.4. (η^4-1,5-Cyclooctadiene)-bis(1,3-dimethylimidazoline-2-ylidene)-iridium (I) iodide (3)

Anal. Calc. for C$_{18}$H$_{28}$/N$_4$Ir (619.572): C 34.89, H 4.55, N 9.04, I 20.48. Found: C 36.41, H 5.08, N 8.49, I19.19, Cl 0%. Calc. including 1/3 hexane (C$_{18}$H$_{28}$IN$_4$Ir · 1/3C$_6$H$_{14}$): C 35.51, H 4.54, N 8.95, I 20.28.

^{1}H NMR (CD$_2$Cl$_2$, 25 °C): $\delta = 7.04$ (s, 4H, NCHCHN), 3.91 (s, 12H, NCH$_3$), 3.82 (s, 4H, CH$_{cod}$), 2.27 (m, 4H, CH$_{2cod}$), 1.95 (m, 4H, CH$_{2cod}$).

^{13}C NMR (CD$_2$Cl$_2$, 25 °C): $\delta = 177.8$ (NCN), 123.2 (NCHCHN), 76.6 (CH$_{cod}$), 38.4 (NCH$_3$), 31.6 (CH$_{2cod}$). MS (FAB; m/z): 493 [cation of 3] (correct isotopic pattern).

4.5. (η^4-1,5-Cyclooctadiene)-bis(1,3-dicyclohexylimidazoline-2-ylidene)-iridium(I) chloride (4)

Anal. Calc. for C$_{38}$H$_{60}$ClN$_4$Ir (800.593): C 57.01, H 7.55, N 7.00, Cl 4.43. Found: C 56.51, H 7.50, N 6.67, Cl.4.43.

^{1}H NMR (CD$_2$Cl$_2$, 25 °C): $\delta = 7.17$ (s, 4H, NCHCHN), 4.67 (m, 4H, CH$_{cod}$), 3.93. (br, 4H, CH$_{cy}$), 2.40–1,20 (m, 48H, CH$_{2cy}$ und CH$_{2cod}$).

^{13}C NMR (CD$_2$Cl$_2$ 25 °C): $\delta = 174.7$ (NCN), 119.4 (NCHCHN), 74.5 (CH$_{cod}$). 60.1 (CH$_{cy}$), 36.2, 34.1, 32.5, 25.9, 25.7, 25.2 (CH$_{2cy}$ and CH$_{2cod}$).

MS (FAB; m/z): 765 [cation of 4] (correct isotopic pattern), 233 [carbene + H$^+$].

4.6. (η^4-1,5-Cyclooctadiene)-(1,3-dimethylimidazoline-2-ylidene)-(η^1-cyclopentadienyl)-iridium(I) (5)

A solution of 500 mg (0.96 mmol) (η^4-1,5-cyclooctadiene)-(1,3-dimethylimidazoline-2-ylidene)-iridium(I) iodide (1) in 25 mL THF, cooled in an ice bath, was treated with a solution of 135 mg (1.53 mmol) of NaC$_5$H$_5$ in 10 mL THF added dropwise. The resulting mixture is warmed to 25 °C and left stirring for 12 h. The solvent is then evaporated in vacuum, the residue extracted with CH$_2$Cl$_2$ and the extract is evaporated to dryness. Yield: 395 mg (89.6%).

Anal. Calc. for $C_{18}H_{25}N_2Ir.1/4CH_2Cl_2$ (482.863): C 45.39, H 5.32, N 5.80. Found: C 45.33, H 5.28, N 5.49.

^{1}H NMR (CD$_2$Cl$_2$, 25 °C): δ = 6.58 (s, 2H, NCHCHN), 5.64 (s, 5H, C$_5$H$_5$), 4.31 (m, 2H, CH$_{cod}$), 3.69 (s, 6H, NCH$_3$), 2.81 (m, 2H, CH$_{cod}$), 2.24 (m, 2H, CH$_{2cod}$), 2.06 (m, 2H, CH$_{2cod}$), 1.75 (m, 2H, CH$_{2cod}$), 1.54 (m, 2H, CH$_{2cod}$).

^{13}C NMR (CD$_2$Cl$_2$, 25 °C): δ = 186.5 (NCN), 121.7 (NCHCHN), 109.1 (C$_5$H$_5$), 77.7 (CH$_{cod}$), 51.4 (CH$_{cod}$), 38.8 (NCH$_3$), 33.5 (CH$_{2cod}$), 31.4 (CH$_{2cod}$).

4.7. $(\eta^2$-1,5-Cyclooctadiene)-(1,3-cyclohexylimidazoline-2-ylidene)-$(\eta^5$-cyclopentadienyl)-iridium(I) (7)

A solution of 0.88 mmol $(\eta^4$-1,5-cyclooctadiene)(1,3-dicyclohexylimidazoline-2-ylidene)-iridium(I) chloride (2) in 20 mL THF, cooled in an ice bath, was treated with a solution of 78 mg (0.88 mmol) in 10 mL THF added dropwise. The resulting mixture is warmed to 25 °C and left stirring for 12 h. The solvent is then evaporated in vacuum, the residue extracted with CH$_2$Cl$_2$, and the extract is evaporated to dryness.

^{1}H NMR (CD$_2$Cl$_2$, 25 °C): δ = 6.76. (s, 2H, NCHeHN), 5.68 (m, 2H, CHcy), 5.56 (m, 2H, CH$_{cod}$, uncoordinated), 4.80 (s, 5H, C$_5$H$_5$), 2.43 (m, 2H, CH$_{cod}$, coordinated) (eh or hhcosy), 2.30–1.10 (m, 28H, CH$_{2cod}$ and CH$_{2cy}$).

^{13}C NMR (CD$_2$Cl$_2$, −70 °C): δ = 159.5 (NCN), 131.1 (CH$_{cod}$, uncoordinated), 115.4 (NCHCHN), 76.8 (C$_5$H$_5$), 60.5 (CH$_{cy}$ or CH$_{cod}$, coordinated), 37.6 (CH$_{cy}$ or CH$_{cod}$, coordinated), 34.8, 33.6, 33.0, 32.8, 26.1, 25.8, 25.5 (CH$_{2cod}$ and CH$_{2cy}$).

4.8. General method for the preparation of $(\eta^4$-1,5-cyclooctadiene)-(1,3-dialkylimidazoline-2-ylidene)-$(\eta^1$-indenyl)-iridium(I) (9, 10)

A solution of $(\eta^4$-1,5-cyclooctadiene)-(1,3-dialkylimidazoline-2-ylidene) iridium(I) halide in THF, cooled in an ice bath, is treated by dropwise addition of a THF solution of Na[C$_9$H$_7$]. After warming to 25 °C, the mixture is stirred for 12 h. The solvent is evaporated under vacuum, extracted with CH$_2$Cl$_2$, and the solution obtained is evaporated to dryness.

4.9. $(\eta^4$-1,5-Cyclooctadiene)-$(\eta^1$-indenyl)-(1,3-dimethylimidazoline-2-ylidene)-iridium(I) (9)

Reagents. 462 mg (0.88 mmol) of **1** in 20 mL THF; (0.88 mmol NaC$_9$H$_7$ in 10 mL THF.

^{1}H NMR (CD$_2$Cl$_2$, 25 °C): δ = 7.30 (m, 2H, C$_{5,8}$H or C$_{6,7}$H), 6.89 (m, 1H, C$_2$H), 6.83 (m, 2H, C$_{5,8}$H or C$_{6,7}$H), 6.38 (s, NCHCHN), 5.09 (d, J(H,H), 2H, C$_{1,3}$H), 3.66 (br, 4H, CH$_{cod}$), 3.16 (s, 6H, NCH$_3$), 2.16 (m, 4H, CH$_{2cod}$), 1.70 (m, 4H, CH$_{2cod}$). Coalescence temperature −60 °C for COD.

^{1}H NMR (CD$_2$Cl$_2$, −90 °C): δ = 7.31 (m, 2H, C$_{5,8}$H or C$_{6,7}$H), 6.91 (m, 1H, C$_2$H), 6.86 (m, 2H, C$_{5,8}$H or C$_{6,7}$H),

6.44 (s, NCHCHN), 5.08 (br, 2H, C$_{1,3}$H), 4.48 (br, 2H, CH$_{cod}$), 3.13 (s, 6H, NCH$_3$), 2.81 (br, 2H, CH$_{cod}$), 2.4–1.20 (m, 8H, CH$_{2cod}$).

^{13}C NMR (CD$_2$Cl$_2$ 25 °C): δ = 185.0 (NCN), 144.6 (C$_{4/9}$), 134.3 (C$_2$), 121.0 (C$_{5–8}$), 119.9 (NCHCHN), 88.7 (C$_{1,3}$), 67.1 (br, CH$_{cod}$), 36.9 (NCH$_3$), 32.4 (CH$_{2cod}$).

^{13}C NMR (CD$_2$Cl$_2$, −90 °C): δ = 183.7 (NCN), 143.4 (C$_{4/9}$), 133.8 (C$_2$), 120.4 (C$_{5–8}$), 119.2 (NCHCHN), 75.9 (br, CH$_{cod}$), 67.6 (C$_3$), 56.4 (br, CH$_{cod}$), 36.3 (NCH$_3$), 32.5 (br, CH$_{2cod}$), 31.3 (br, CH$_{2cod}$), 25.4 (C$_1$). At coalescence temperature for COD, ca. −60 °C, (CH$_{1,3}$) signals are already coalesced.

4.10. $(\eta^4$-1,5-Cyclooctadiene)-(1,3-dicyclohexylimidazoline-2-ylidene)-$(\eta^1$-indenyl)iridium(I) (10)

Reagents. 500 mg (0.88 mmol) of **2** in 25 mL THF; 0.88 mmol NaC$_9$H$_7$ in 10 mL THF.

^{1}H NMR (THF-d_8, 25 °C, ppm): δ = 7.27 (m, 2H, C$_{5,8}$H or C$_{6,7}$H), 7.06 (s, 6.82 (m, 2H, C$_{5,8}$H or C$_{6,7}$H), 6.67 (m, 1H, C$_2$H), 5.48 (d, 2H, C$_{1,3}$H), 5.00 (m, 2H, CH$_{cy}$), 3.05 (br, 4H, CH$_{cod}$), 2.30–0.80 (m, 28H, CH$_{2cod}$ and CH$_{2cy}$. Coalescence temperature −20 °C for (CH$_{cod}$).

^{1}H NMR (THF-d_8, −50 °C, ppm): δ = 7.27 (m, 2H, C$_{5,8}$H or C$_{6,7}$H), 7.20 (s, NCHCHN), 6.83 (m, 2H, C$_{5,8}$H or C$_{6,7}$H), 6.65 (m, 1H, C$_2$H), 5.52 (br, 2H, C$_{1,3}$H), 5.02 (m, 2H, CH$_{cy}$), 3.02 (br, 2H, CH$_{cod}$), 2.90 (br, 2H, CH$_{cod}$), 2.30–0.80 (m, 28H, CH$_{2cod}$ and CH$_{2cy}$). Turning point: −50 °C.

^{1}H NMR (THF-d_8, −100 °C, ppm): δ = 7.27 (s, NCHCHN), 7.25 (m, 2H, C$_{5,8}$H or C$_{6,7}$H), 6.84 (m, 2H, C$_{5,8}$H or C$_{6,7}$H), 6.63 (m, 1H, C$_2$H), 5.54 (very br, 2H, C$_{1,3}$H), 5.03 (m, 2H, CH$_{cy}$), 2.89 (br, 4H, CH$_{cod}$), 2.30–0.80 (m, 28H, CH$_{2cod}$ and CH$_{2cy}$).

^{13}C NMR (CD$_2$Cl$_2$, 35 °C): δ = 182.5 (NCN), 148.9 (C$_{4/9}$), 136.8 (C$_2$), 121.4 (C$_{5,8}$), 121.0 (C$_{6,7}$), 118.2 (NCHCHN), 87.0 (br, C$_{1,3}$), 60.8 (CH$_{2cy}$), 36.3, 34.7, 30.5, 27.0, 26.4 (CH$_{2cy}$), 32.3 (br, CH$_{2cod}$). Coalescence temperature for COD 35 °C.

^{13}C NMR (CD$_2$Cl$_2$, 25 °C): δ = 185.0 (NCN), 148.9 (C$_{4/9}$), 136.6 (C$_2$), 121.3 (C$_{5,8}$). 121.0 (C$_{6,7}$), 118.3 (NCHCHN), 86.8 (br, C$_{1/3}$), 79.2 (br, CH$_{cod}$), 60.7 (CH$_{2cy}$), 57.8 (br, CH$_{cod}$), 36.2, 34.6, 27.0, 26.4 (CH$_{2cy}$), 32.3 (br, CH$_{2cod}$). Coalescence temperature for CH$_{1,3}$ −50 °C.

^{13}C NMR (CD$_2$Cl$_2$, −50 °C): δ = 181.5 (NCN), 148.8 (br, C$_{4/9}$), 136.2 (C$_2$), 121.3, (C$_{5,8}$), 120.9 (C$_{6,7}$), 118.5 (NCHCHN), 79.0 (br, CH$_{cod}$), 60.6 (CH$_{2cy}$), 57.4 (br, CH$_{cod}$), 57.8 (br, CH$_{cod}$), 36.0, 34.5, 26.9, 26.3 (shoulder) 5, 31.1 (CH$_{2cod}$).

^{13}C NMR (CD$_2$Cl$_2$, −100 °C): δ = 181.0 (NCN), 148.3 (very broad and flat, C$_{4/9}$), 135.8 (C$_2$), 121.3 (C$_{5,8}$), 120.9 (C$_{6,7}$), 118.7), 118.7 (NCHCHN), 79.2 (br, CH$_{cod}$), 60.5 (CH$_{2cy}$), 57.2 (br, CH$_{cod}$), 35.9, 34.5, 26.9, 26.4, 26.2 (CH$_{2cy}$), 33.5, 31.1 (CH$_{2cod}$).

4.11. Single crystal X-ray structure determination of compounds 1, 5, 7, and 10 · (CH₂Cl₂)

Crystal data and details of the structure determination are presented in Table 5. Suitable single crystals for the X-ray diffraction study were grown by slow diffusion of *n*-hexane in saturated solutions of compounds **1**, **5**, **7**, and **10** in CH_2Cl_2. Crystals were stored under perfluorinated ether, transferred in a Lindemann capillary, fixed, and sealed. Preliminary examination and data collection were carried out on an area detecting system (NONIUS, MACH3, κ-CCD) at the window of a rotating anode (NONIUS, FR591) and graphite monochromated Mo Kα radiation ($\lambda = 0.71073$ Å). Data collection were performed at 123 (173, 173, 173) K (OXFORD CRYOSYSTEMS) within a θ-range of $2.36° < \theta < 25.38°$ ($2.98° < \theta < 27.50°$, $1.83° < \theta < 25.39°$, $2.14° < \theta < 27.48°$). Measured with ten (four, three, two) data sets in rotation scan modus with $\Delta\varphi/\Delta\omega = 1.0°$. A total number of 32 693 (16 473, 13 938, 13 048) intensities were integrated. Raw data were corrected for Lorentz, polarization, and, arising from the scaling procedure, for latent decay. Absorption effects were corrected with the PLATON DELABS procedure. After merging [$R_{int} = 0.057$ (0.052, 0.054, 0.031)] a sum of 2625 (3636, 4702, 6815) (all data) and 2623 (2854, 4646, 6058) [$I > 2\sigma(I)$], respectively, remained and all data were used. The structures were solved by a combination of direct methods and difference Fourier syntheses. All

non-hydrogen atoms were refined with anisotropic displacement parameters. All hydrogen atoms were placed in ideal positions (riding model). Full-matrix least-squares refinements with 155 (192, 281, 343) parameters were carried out by minimizing $\sum w(F_o^2 - F_c^2)^2$ with the SHELXL-97 weighting scheme and stopped at shift/err < 0.002. The relatively high final residual electron density peaks are located near the heavy atoms I and Ir and are caused by an incomplete absorption correction due to the irregular shape of the crystals. Neutral atom scattering factors for all atoms and anomalous dispersion corrections for the non-hydrogen atoms were taken from *International Tables for Crystallography*. All calculations were performed on an Intel Pentium II PC, with the STRUX-V system, including the programs PLATON, SIR-92, and SHELXL-97 [22]. **1**: Small extinction effects were corrected with the SHELXL-97 formalism [($x = 0.0051(2)$]. **7**: As shown by Flack's parameter $\varepsilon = 0.484(12)$ the crystal appears to be twinned. The problem was solved with the SHELXL-97 TWIN/BASF procedure. Crystallographic data (excluding structure factors) for the structures reported in this paper have been deposited with the Cambridge Crystallographic Data Centre as supplementary publication no. CCDC-295611 (**1**), CCDC-295612 (**5**), CCDC-295613 (**7**), and CCDC-295614 [**10** · (CH_2Cl_2)]. Copies of the data can be obtained free of charge on application to CCDC, 12 Union Road, Cambridge CB2 1EZ, UK (fax: +44 1223 336 033; e-mail: deposit@ccdc.cam.ac.uk).

Table 5
Crystallographic Data for compounds **1**, **5**, **7**, and **10** · (CH₂Cl₂)

	1	5	7	10 · (CH₂Cl₂)
Formula	C₁₃H₂₀IIrN₂	C₁₈H₂₅IrN₂	C₂₈H₄₁IrN₂	C₃₃H₄₅Cl₂IrN₂
F_w	523.43	461.62	597.85	732.83
Color/habit	Pale brown/fragment	Pale brown/fragment	Pale brown/fragment	Pale brown/plate
Crystal dimensions (mm³)	0.34 × 0.42 × 0.47	0.25 × 0.32 × 0.39	0.18 × 0.51 × 0.64	0.05 × 0.25 × 0.48
Crystal system	Monoclinic	Orthorhombic	Orthorhombic	Monoclinic
Space group	$P2_1/n$ (no. 14)	$Pbca$ (no. 61)	$P2_12_12_1$ (no. 19)	$P2_1/c$ (no. 14)
a (Å)	9.5666(1)	7.176(2)	10.1185(1)	12.911(1)
b (Å)	13.0507(1)	13.677(3)	14.2311(3)	10.523(2)
c (Å)	11.9100(1)	33.164(9)	17.9058(3)	22.577(1)
β (°)	105.4854(6)	90	90	94.508(1)
V (Å³)	1432.99(2)	3254.9(15)	2578.39(7)	3057.9(6)
Z	4	8	4	4
T (K)	123	173	173	173
D_{calc} (g cm⁻³)	2.426	1.884	1.540	1.592
μ (mm⁻¹)	11.453	8.200	5.195	4.566
$F(000)$	968	1792	1200	1472
θ Range (°)	2.36–25.38	2.98–27.50	1.83–25.39	2.14–27.48
Index ranges (h,k,l)	±11, ±15, ±14	±9, ±17, ±43	±12, ±17, ±21	±16, ±13, ±29
No. of reflections collected	32 693	16 473	13 938	13 048
No. of independent reflections/R_{int}	2625/0.057	3636/0.052	4702/0.054	6815/0.031
No. of observed reflections ($I > 2\sigma(I)$)	2623	2854	4646	6058
No. of data/restraints/parameters	2625/0/155	3636/0/192	4702/0/281	6815/0/343
R_1/wR_2 ($I > 2\sigma(I)$)[a]	0.0209/0.0534	0.0385/0.0787	0.0266/0.0619	0.0458/0.1192
R_1/wR_2 (all data)[a]	0.0209/0.0535	0.0519/0.0829	0.0271/0.0622	0.0510/0.1234
GOF (on F^2)[a]	1.214	1.109	1.052	1.040
Largest diff peak and hole (e Å⁻³)	+1.37 /−0.97	+2.01/−1.27	+1.06/−1.38	+5.52/−2.63

[a] $R_1 = \sum(||F_o| - |F_c||/\sum|F_o|$; $wR_2 = \{\sum[w(F_o^2 - F_c^2)^2]/\sum[w(F_o^2)^2]\}^{1/2}$; GOF $= \{\sum[w(F_o^2 - F_c^2)^2]/(n-p)\}^{1/2}$.

5. Computational details

DFT calculations were performed with the GAUSSIAN 98 program [23]. The B3LYP hybrid functional was used. It includes a mixture of Hartree–Fock [24] exchange with DFT [10] exchange-correlation, given by Becke's three parameter functional [25] with the Lee, Yang and Parr correlation functional, which includes both local and non-local terms [26,27]. All the geometries were fully optimized without any symmetry constraints. The Cy and Me substituents on the *N*-heterocycle carbene were replaced by hydrogen atoms in order to save computational time. A LanL2DZ [28,29] basis set with an added f-polarization function [30] was used for Ir, and a standard D95 [28] basis set was employed for C, N and H.

Acknowledgements

References

[1] (a) J.M. O'Connor, C.P. Casey, Chem. Rev. 87 (1987) 307;
(b) M.J. Calhorda, V. Félix, L.F. Veiros, Coord. Chem. Rev. 230 (2002) 49.

[2] F.H. Allen, Acta Crystallogr. B58 (2002) 380–388.

[3] M.J. Calhorda, C.C. Romão, L.F. Veiros, Chem. Eur. J. 8 (2002) 868–875.

[4] M.E. Rerek, L.-N. Ji, F. Basolo, J. Chem. Soc., Chem. Commun. (1983) 1208.

[5] M.J. Calhorda, C.A. Gamelas, I.S. Gonçalves, E. Herdtweck, C.C. Romão, L.F. Veiros, Organometallics 17 (1998) 2597.

[6] M.J. Calhorda, C.A. Gamelas, C.C. Romão, L.F. Veiros, Eur. J. Inorg. Chem. 331 (2000).

[7] (a) M.J. Calhorda, L.F. Veiros, Coord. Chem. Rev. 185–186 (1999) 37;
(b) M.J. Calhorda, L.F. Veiros, Comment Inorg. Chem. 22 (2001) 375.

[8] L.F. Veiros, Organometallics 19 (2000) 3127.

[9] M. Straditto, M.J. McGlinchey, Coord. Chem. Rev. 219–221 (2001) 311.

[10] R.G. Parr, W. Yang, Density Functional Theory of Atoms and Molecules, Oxford University Press, New York, 1989.

[11] (a) M. Prinz, Diploma Thesis, Technische Universität München, 1997;
(b) C. Köcher, W.A. Herrmann, J. Organomet. Chem. 532 (1997) 261;
(c) L.J. Gooßen, Ph.D. Thesis, Technische Universität München, 1997.

[12] C. Köcher, Ph.D. Thesis, Technische Universität München, 1997.

[13] (a) P. Burger, R.G. Bergman, J. Am. Chem. Soc. 115 (1993) 10462;
(b) B.A. Arndtsen, R.G. Bergman, Science 270 (1995) 1970;

[14] R.T. Baker, T.H. Tulip, Organometallics 5 (1986) 839.

[15] J.S. Merola, R.T. Kacmarcik, D. Van Engen, J. Am. Chem. Soc. 108 (1986) 329.

[16] L.F. Veiros, J. Organomet. Chem. 587 (1999) 221.

[17] T.A. Albright, J.K. Burdett, M.H. Whangbo, Orbital Interactions in Chemistry, John Wiley & Sons, New York, 1985.

[18] L.F. Veiros, Organometallics 19 (2000) 5549.

[19] X. Zheng, G.E. Herberich, Organometallics 19 (2000) 3751.

[20] J.C. Green, R.G. Scurr, P.L. Arnold, F.G.N. Cloke, Chem. Commun. (1997) 1963.

[21] A.B. Pangborn, M.A. Giardello, R.H. Grubbs, R.K. Rosen, F.J. Timmers, Organometallics 15 (1996) 1518.

[22] (a) Data Collection Software for Nonius κ-CCD devices, Delft, The Netherlands, 2001;
(b) Z. Otwinowski, W. Minor, Methods Enzymol 276 (1997) 307ff;
(c) A. Altomare, G. Cascarano, C. Giacovazzo, A. Guagliardi, M.C. Burla, G. Polidori, M. Camalli, J. Appl. Crystallogr. 27 (1994) 435–436;
(d) A.J.C. Wilson (Ed.), International Tables for Crystallography, vol. C, Kluwer Academic Publishers, Dordrecht, The Netherlands, 1992, Tables 6.1.1.4, 4.2.6.8, and 4.2.4.2;
(e) G.M. Sheldrick, SHELXL-97, Universität Göttingen, Göttingen, Germany, 1998;
(f) A.L. Spek, PLATON, A Multipurpose Crystallographic Tool, Utrecht University, Utrecht, The Netherlands, 2001.

[23] M.J. Frisch, G.W. Trucks, H.B. Schlegel, G.E. Scuseria, M.A. Robb, J.R. Cheeseman, J.A. Montgomery Jr., T. Vreven, K.N. Kudin, J.C. Burant, J.M. Millam, S.S. Iyengar, J. Tomasi, V. Barone, B. Mennucci, M. Cossi, G. Scalmani, N. Rega, G.A. Petersson, H. Nakatsuji, M. Hada, M. Ehara, K. Toyota, R. Fukuda, J. Hasegawa, M. Ishida, T. Nakajima, Y. Honda, O. Kitao, H. Nakai, M. Klene, X. Li, J.E. Knox, H.P. Hratchian, J.B. Cross, C. Adamo, J. Jaramillo, R. Gomperts, R.E. Stratmann, O. Yazyev, A.J. Austin, R. Cammi, C. Pomelli, J.W. Ochterski, P.Y. Ayala, K. Morokuma, G.A. Voth, P. Salvador, J.J. Dannenberg, V.G. Zakrzewski, S. Dapprich, A.D. Daniels, M.C. Strain, O. Farkas, D.K. Malick, A.D. Rabuck, K. Raghavachari, J.B. Foresman, J.V. Ortiz, Q. Cui, A.G. Baboul, S. Clifford, J. Cioslowski, B.B. Stefanov, G. Liu, A. Liashenko, P. Piskorz, I. Komaromi, R.L. Martin, D.J. Fox, T. Keith, M.A. Al-Laham, C.Y. Peng, A. Nanayakkara, M. Challacombe, P.M.W. Gill, B. Johnson, W. Chen, M.W. Wong, C. Gonzalez, J.A. Pople, GAUSSIAN 03, Revision C.02, Gaussian, Inc., Wallingford, CT, 2004.

[24] W.J. Hehre, L. Radom, P.v.R. Schleyer, J.A. Pople, Ab Initio Molecular Orbital Theory, John Wiley & Sons, NY, 1986.

[25] A.D. Becke, J. Chem. Phys. 98 (1993) 5648.

[26] C. Lee, W. Yang, R.G. Parr, Phys. Rev. B 37 (1988) 785.

[27] B. Miehlich, A. Savin, H. Stoll, H. Preuss, Chem. Phys. Lett. 157 (1989) 200.

[28] T.H. Dunning Jr., P.J. Hay, in: H.F. SchaeferIII (Ed.), Modern Theoretical Chemistry, vol. 3, Plenum, New York, 1976, p. 1.

[29] (a) P.J. Hay, W.R. Wadt, J. Chem. Phys. 82 (1985) 270;
(b) W.R. Wadt, P.J. Hay, J. Chem. Phys. 82 (1985) 284;
(c) P.J. Hay, W.R. Wadt, J. Chem. Phys. 82 (1985) 2299.

[30] A.W. Ehlers, M. Böhme, S. Dapprich, A. Gobbi, A. Höllwarth, V. Jonas, K.F. Köhler, R. Stegmann, A. Veldkamp, G. Frenking, Chem. Phys. Lett. 208 (1993) 111.